JOURNAL OF SOLID STATE CHEMISTRY 113, 94–108 (1994)

Structural Aspects and Antiferromagnetic Ordering in the "123" Derivative $LnSr_2Cu_2Ga_{1-x}Fe_xO_{7-\delta}$ (Ln = Y, Ho)

A. Rykov,[1] V. Caignaert, G. Van Tendeloo,[2] J. M. Greneche,[3] F. Studer, N. Nguyen, A. Ducouret, P. Bonville,[4] and B. Raveau

Laboratoire CRISMAT, CNRS URA 1318, ISMRA, Université de Caen, 14050 Caen Cedex, France

Received November 18, 1993; accepted February 4, 1994

The magnetic ordering in the orthorhombic phases $LnSr_2Cu_2Ga_{1-x}Fe_xO_7$ (Ln = Y, Ho; $0.03 \leq x \leq 0.95$) has been investigated by ^{57}Fe Mössbauer spectroscopy. Iron occupies the Ga site (Cu(1) site) for small doping rates ($x \approx 0.03$), but occupies the Cu(1) and Cu(2) sites for iron-rich compositions ($0.5 \leq x \leq 0.95$). For x = 0.9, the magnetic ordering takes place below $T_N \approx 420$ K in both the Cu(1) and Cu(2) sites. The down concave curve of the temperature dependence of the hyperfine field in the Cu(1) site suggests a rather weak coupling between the Cu(1) and Cu(2) sites. The principal EFG axis V_{ZZ} is directed in both sites along the longest axis of the orthorhombic cell, i.e., perpendicular to the alternating sheets. The sign of V_{ZZ} is positive for the Cu(2) sites (ΔE_Q = 0.6 mm/sec) and negative for the Cu(1) sites (ΔE_Q = −1.9 mm/sec). In the distorted tetrahedral site, the EFG tensor is non-axial, however, its asymmetry is small ($\eta < 0.4$). The magnetic hyperfine field is perpendicular to the V_{ZZ} axis for both sites; i.e., H lies in the plane of the shortest axes. A structural analysis by electron microscopy reveals the presence of a large number of defects in the (Fe, Ga)O chain ordering as well as in the basic structure. The presence and the abundance of these defects is in agreement with the Mössbauer observations.

1. INTRODUCTION

The study of the magnetic interactions in high-T_c superconductors is important for understanding the mechanism of superconductivity. Mössbauer spectroscopy is one of the effective methods used to investigate the delicate interplay between superconductivity and magnetism. In a number of ^{57}Fe-doped high-T_c superconductors, the magnetic order has been observed by Mössbauer spectroscopy to be induced either by oxygen depletion or by Fe-substitution (see (1–4) and Refs. therein). Superconductivity is suppressed in both of these conditions due to the removal of the doping holes from the copper planes, so that copper atoms become involved in the concurrent phenomenon of antiferromagnetic ordering. In particular, for $YBa_2Cu_3O_6$, the antiferromagnetic ordering in the Cu(2) planes at the critical temperature T_N of about 420 K is fairly well detected by the Mössbauer probe ^{57}Fe substituted on the Cu(2) sites. Generally, the T_N value in the parent "undoped" compounds is weakly dependent on the concentration of impurity atoms, substituted into copper sites, but it decreases very rapidly by doping the system by holes in the course of the oxygenation or by substituting Ca for Y in $YBa_2Cu_3O_6$, or Sr for La in La_2CuO_4; see, e.g., (5). Both T_N and T_c values in the parent and hole-doped compounds, respectively, are thought to be characteristic of CuO_2 planes either isolated from each other or incorporated in blocks of two, three, or more layers.

The double pyramidal Cu(2) layers may be regarded as the leading structural elements, ensuring both superconducting and magnetic properties of the "123"-related cuprates. In the desoxygenated $YBa_2Cu_{3-x}Fe_xO_{6+y}$, the coupling between the Cu(2) and the Cu(1) sites is rather weak; this leads to a competition of magnetic order with different stacking of the antiferromagnetic sheets along the c-axis (6, 7). The magnetic moment induced on the Cu(1) site by impurity atoms can be coupled either antiferro- or ferromagnetically with adjacent Cu(2) sheets (see (7) and Refs. therein). With respect to copper, Fe(III) occupying the Cu(1) level, is susceptible to attract some extra oxygen, owing to its higher oxidation state. The excess of oxygen with respect to the "O_6" stoichiometry is known to induce the magnetic moment at these sites; this makes it difficult to distinguish the effect of iron doping from the effect of oxygen excess on the magnetic order.

The system $LnSr_2Cu_2GaO_7$, structurally related to the 123 superconductor, provides another example for studying the magnetism of Cu(2) bilayers. As in $YBa_2Cu_3O_6$,

[1] On sabbatical leave from the Institute of Solid State Chemistry, Siberian Branch of the Russian Academy of Sciences, Novosibirsk 630090, Russia.

[2] On leave from the University of Antwerp (RUCA) Groenenborgerlaan 171, B-2020 Antwerpen, Belgium.

[3] Equipe de Physique de l'Etat Condensé, Laboratoire de Physique de Materiaux, U.A. 807, 72017, Le Mans Cedex, France

[4] Service de Physique de l'Etat Condensé, DRECAM, Centre d'Etudes Nucléaires de Saclay, 91191 Gif-Sur-Yvette Cedex, France

0022-4596/94 $6.00

TABLE 1
Crystallographic Parameters of the Samples of $LnSr_2Cu_2Ga_{1-x}Fe_xO_{7-\delta}$

Ln	Ho	Ho	Ho	Y	Y
x	0.03	0.9	0.9	0.8	0.8
Treatment	$[O_{sc}]$	$[Ar_{fc}]$	$[Ar_{sc}]$	$[Ar_{fc}]$	$[ArO_{LT}Ar_{LT}]$
δ	0.0(1)	0.0(1)	0.0(1)	0.0(1)	0.1(1)
a_s(Å)	5.4779(2)	5.4593(3)	5.4598(3)	5.4646(3)	5.4576(3)
b_s(Å)	10.7882(5)	10.8148(7)	10.8140(7)	10.8184(8)	10.8132(7)
c_s(Å)	22.811(1)	22.910(1)	22.904(1)	22.912(2)	22.886(2)
V(Å^3)	674.0(1)	676.3(1)	676.1(1)	677.2(1)	675.3(1)

the Cu(2) bilayers in this system are separated by diamagnetic Ga sites. The structure is orthorhombic due to the formation of zigzag chains of GaO_4 tetrahedra running along the diagonal of the basal plane (8, 9). The similarity between the magnetic structures of $YBa_2Cu_3O_6$ and of $LnSr_2Cu_2GaO_7$ has been suggested from the studies of Ga and Cu NMR/NQR in $LnSr_2Cu_2GaO_7$ (10).

The objective of this work is to introduce magnetic Fe–O chains in-between the Cu(2) layers to examine the magnetism resulting from interactions of the Cu(2) layers with the zigzag FeO chains. The compounds of the system $LnSr_2Cu_2FeO_7$–$LnSr_2Cu_2GaO_7$ have been prepared under different oxygenating conditions (O_2 and Ar flow). Their previous Mössbauer study at room temperature provided evidence of the tetrahedral coordination for Fe(III) substituted into the Ga site (11). The previous studies of the end member in this series $YSr_2Cu_2FeO_y$ ($6.8 < y < 7.5$) (12, 13) have shown that the magnetism of the Cu(2) bilayer in this compound is strongly influenced by a hole transfer from the $Cu(1)O_y$ planes. The Néel temperature of $YSr_2Cu_2FeO_{7.26}$ (13) is as low as 65K (13), to be compared with a T_N of 420 K in $YBa_2Cu_{2.3}Fe_{0.7}O_{7.21}$ (3). We have shown that subtle doping of this compound by Ga allows to stabilize an orthorhombic structure in $LnSr_2Cu_2Ga_{1-x}Fe_xO_7$ even for $x = 0.95$ (11). In this structure, the oxygen stoichiometry is fixed to the value of 7.0 since the oxygen atoms of the Cu(1) layer are incorporated into the chains of FeO_4 (GaO_4) tetrahedra running along the diagonal of the basal plane of the 123 unit cell. Moreover, it has been shown (11) that for $0.05 \leq x \leq 0.4$ the orthorhombic form $LnSr_2Cu_2Fe_{1-x}Ga_xO_7$ can be oxidized in a tetragonal form $LnSr_2Cu_2Fe_{1-x}Ga_xO_{7+\delta}$, depending on the oxidizing conditions. Specifically, by heating the tetragonal form in an Ar flow the extra oxygen atoms are removed from the Cu(1) level, so that the FeO_4 tetrahedra form ordered chains characteristic of the orthorhombic structure.

2. EXPERIMENTAL

The two important compositions for the magnetic study of $LnSr_2Cu_2Ga_{1-x}Fe_xO_7$ are the $x = 0$ and $x = 1$ compounds that correspond to full occupancy of the Cu(1) site by diamagnetic Ga or strongly magnetic Fe ions. The samples with nominal compositions $HoSr_2Cu_2Fe_{0.03}Ga_{0.97}O_7$, $HoSr_2Cu_2Fe_{0.95}Ga_{0.05}O_7$, $HoSr_2Cu_2Fe_{0.9}Ga_{0.1}O_7$, and $YSr_2Cu_2Fe_{0.8}Ga_{0.2}O_7$ were prepared by standard ceramic techniques. The stoichiometric amounts of Ga_2O_3, $SrCO_3$, CuO, Fe_2O_3, and Y_2O_3 or Ho_2O_3 were thoroughly mixed and ground. The powder was sintered at 950°C in air for about 72 hr with two intermediate grindings and then annealed at 850°C in Ar flow. The as-synthesized samples were divided into several parts; the aliquots of samples were subjected further to different treatments in O_2 flow and in Ar flow as described previously (11). In order to check the influence of subtle variations in the oxygen content on the cationic distribution and magnetic properties of the Cu(2)-layers, the preparation conditions in Ar flow were modified as follows:

—$[Ar_{fc}]$: annealing at 850°C in flowing Ar gas for 36 hr and fast cooling (furnace cooling) to room temperature in Ar. $[Ar_{sc}]$: annealing at 850°C in flowing Ar gas for 36 hr and slow cooling (50°/hr) in Ar.

—$[ArO_{LT}Ar_{LT}]$: the treatment $[Ar_{fc}]$ followed by oxygenation in oxygen flow at relatively low temperature ("LT" = 400°C) then by reduction in Ar flow, again at low temperature. This treatment allowed to prepare orthorhombic samples with some excess of oxygen with respect to "O_7" stoichiometry.

The oxygen content has been evaluated from the combination of X-ray and thermogravimetric measurements. These data are given in the Table 1, together with the lattice parameters. Note that no difference between oxygen content in the $[Ar_{fc}]$ and $[Ar_{sc}]$ samples was detected.

The powder X-ray diffraction data at room temperature were collected by step scanning over an angular range 22–102°(2θ) with increment 0.02°(2θ) with a high-resolution diffractometer "SEIFERT" using Cu $K_{\alpha 1}$ radiation. The full diffraction profiles were analyzed by the Rietveld method.

Electron microscopy was performed on a TOPCON 0002B instrument operating at 200 kV and having a point resolution of 1.8 Å.

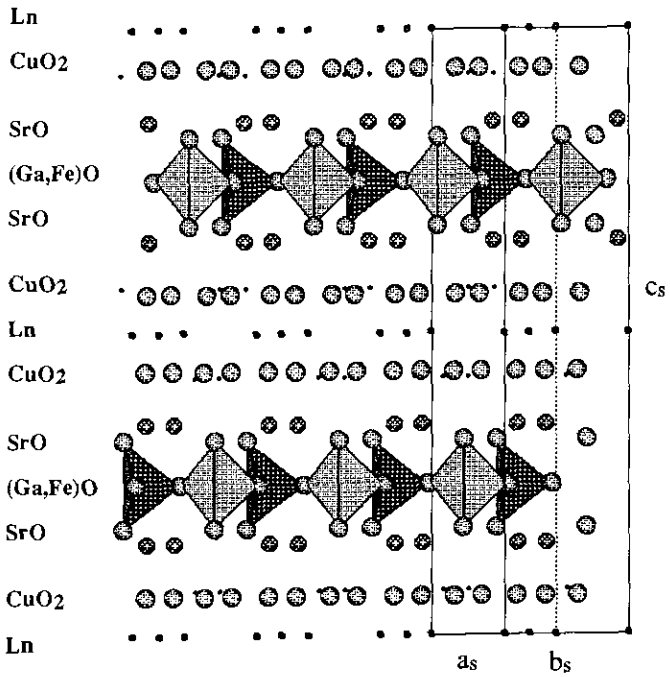

FIG. 1. The chains of $GaO_4(FeO_4)$ tetrahedra in the structure of $LnSr_2Cu_2(Ga, Fe)O_7$, projected along the $[110]_s$ axis.

Mössbauer spectra were recorded at room temperature using a constant-acceleration spectrometer in the time mode and a 512-channel analyzer. Velocity scale calibration and isomer shift reference point were obtained by the room-temperature measurement of the spectra of an α-^{57}Fe foil.

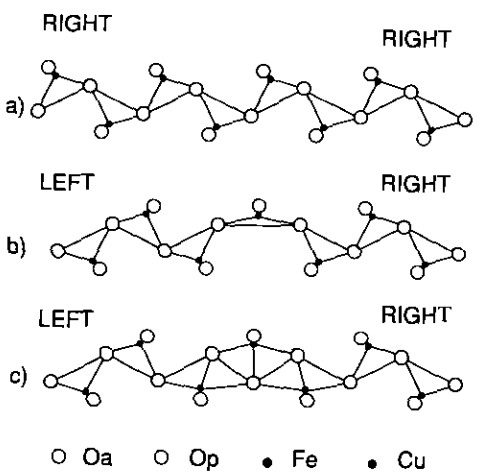

FIG. 2. Schematic representation of the *MO* chains in the (001) layer. (a) A "right" chain without defect. (b) The change in the chain orientation from "left" to "right" induced by the presence of a copper ion in the (Fe, Ga)-sublattice. (c) The change in the chain orientation from "left" to "right" induced by the presence of an extra oxygen atom at the level of the (Fe, Ga)-site.

3. RESULTS AND DISCUSSION

3.1. Structural Considerations

It was shown recently that metallic ions such as Ga, Co, Fe, or Al can be substituted for the copper sites in the $Cu(1)O_y$ layer of the "123"-type structures (8, 9, 11–17). The above cations tend to be tetrahedrally coordinated by oxygen, rather than adopting the square planar CuO_4 configuration. Without changing the main features of the "123" structure, such substitutions give rise to interesting superstructures due to the different arrangements of the MO_4 tetrahedra in the Cu–O layer.

In $YSr_2Cu_2GaO_7$, as well as in all related compounds, the MO_4 tetrahedra are corner-linked and form chains (Fig. 1). In the Ga and Co compounds the "zigzag" chains are oriented along the $[110]_{123}$ and $[1\bar{1}0]_{123}$ directions (8, 9, 14, 15), whereas in the Al-containing compound the average direction of the chains is $[100]_{123}$ or $[010]_{123}$ (16). The structure of $YSr_2Cu_2GaO_7$ have been refined from neutron and X-ray data in the orthorhombic space group *Ima*2 (8, 9) with approximate lattice parameters

$$a_0 \approx 2c_{123} \approx 23\ \text{Å}, \quad b_0 \approx \sqrt{2}a_{123} \approx 5.5\ \text{Å},$$
$$c_0 \approx \sqrt{2}a_{123} \approx 5.4\ \text{Å}.$$

In this description, the chains are running along the b_0-axis. One discerns "left" and "right" rotated chains of corner-linked tetrahedra due to an asymmetry in zigzag

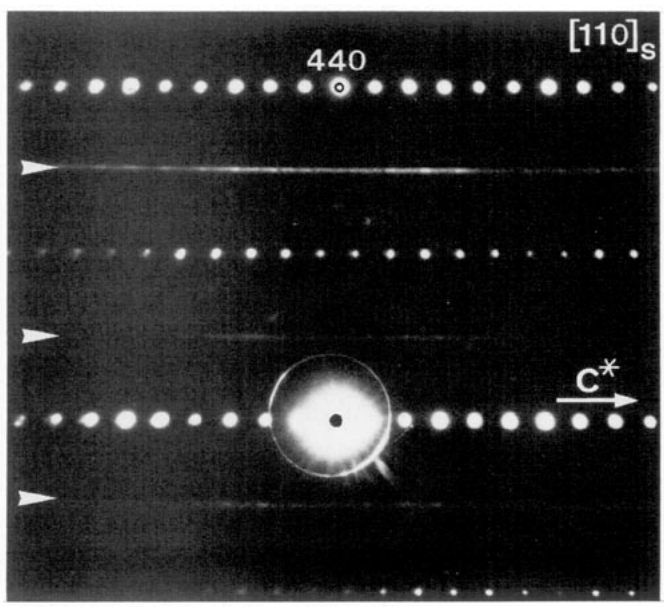

FIG. 3. $[110]_s$ diffraction pattern of $HoSr_2Cu_2(Fe_{0.95}Ga_{0.05})O_{7-\delta}$. Note the diffuse streaking parallel to c^*, passing through the *hhl* reflections with $h = 2n + 1$.

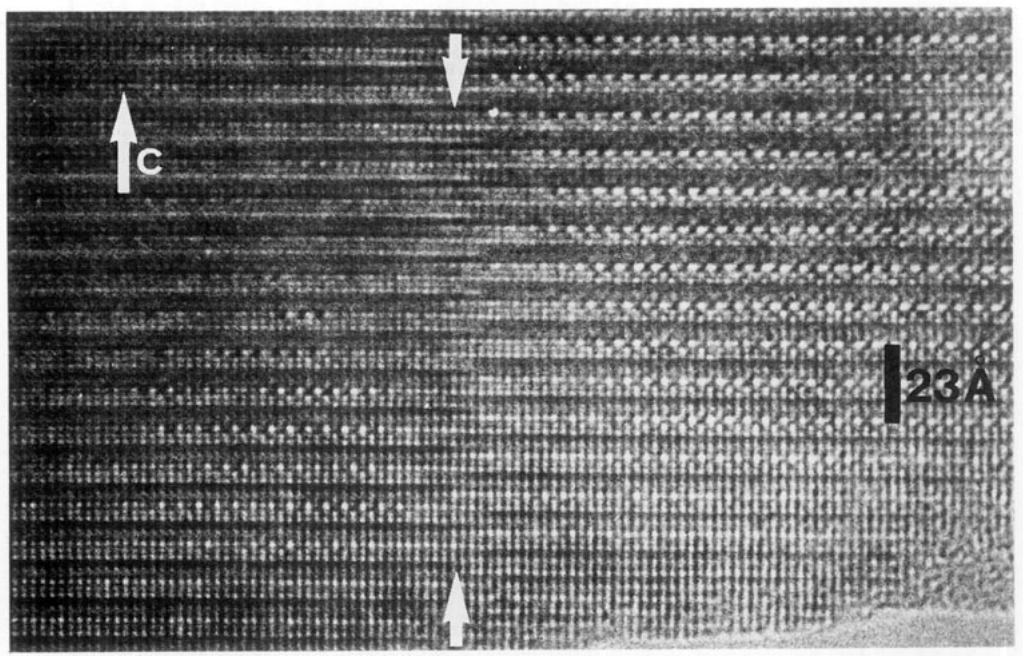

FIG. 4. HREM image along $[010]_s$(or$[100]_s$) for the same compound as in Fig. 3. The Fe–O chains, seen edge on, are imaged as intense bright dots separated by 5.4 Å. In areas where the 5.4 Å superperiod is absent, the chains are rotated over 90° within the same plane. The arrows indicate an antiphase boundary in the basic structure.

buckling (Fig. 2). Electron diffraction and HREM have detected an ordering between these two kinds of chains, which leads to a cell doubling with respect to the above description (15, 16):

$$a_s = 2c_0 \approx 2\sqrt{2}a_{123} \approx 10.8\ \text{Å}, \quad b_s = b_0 \approx \sqrt{2}a_{123} \approx 5.5\ \text{Å},$$
$$c_s \approx 2c_{123} \approx 23\ \text{Å}.$$

The changes in notation with respect to (8, 9) were introduced because the superstructure is B-centered (17). Moreover it is convenient to keep the c-axis parallel to the long axis of the 123 structure; the chains are now running along the b_s-axis.

We have investigated here the $HoSr_2Cu_2(Fe_{0.95}Ga_{0.05})O_{7-\delta}$ compound by electron diffraction and high resolution electron microscopy (HREM). The ordering of "left" and "right" chains is clearly observed in the $[110]_s$ diffraction pattern (Fig. 3). When compared to the diffraction pattern of Fig. 3 in Ref. (15), it is obvious that the two patterns are similar but that in the present case the streaks through the hhl reflections (h = odd) are almost continuous, with only weak periodic reinforcements having the same period as the sharp dot rows. The streaks only pass through the superstructure reflections and suggest that the superstructure is heavily disordered, more than in the Co compound (17). High-resolution images along the $[110]_s$ zone confirmed the observations made in the Co-compound; the two types of chains alternate along the a_s-axis. Disorder and a change from "left"-chain into "right"-chain can be induced by the presence of a Cu-ion in the (Fe, Ga)O plane (Fig. 2b). This means that in the basal plane not only the tetrahedral coordination is present, but, occasionally, also a planar square configuration. When copper is sitting partly in the Cu(1) site, the stoichiometry requires for a fraction of iron atoms to be located in the pyramidal Cu(2) site. This finding has indeed been supported by Mössbauer spectroscopy observations as reported below (Section 3.3).

Along the $[010]_s$ zone, the Fe–O–Fe chains are seen edge on; the HREM image along this zone exhibits bright dots forming a staggered arrangement (Fig. 4). The bright dots are located in the FeO layers and represent the arrangement of the Fe–O–Fe chains; the separation of the chains being 5.4 Å. Similar to the cobalt compound, it is observed that in certain dot rows the spacing changes from 5.4 into 2.7 Å or vice versa (15); this was shown to be due to a change in orientation over 90° of the chains within the same layer.

From these observations we conclude that Fe in the Cu(1)O layer, similarly to Co and Ga-substitutions, gives rise to the formation of a superstructure confined to that layer and consisting of alternating sequences of "zigzag" shaped chains of corner-sharing tetrahedra of two different kinds oriented along $[110]_{123}$ or $[1\bar{1}0]_{123}$ directions.

The two orientations of chains encountered in the mate-

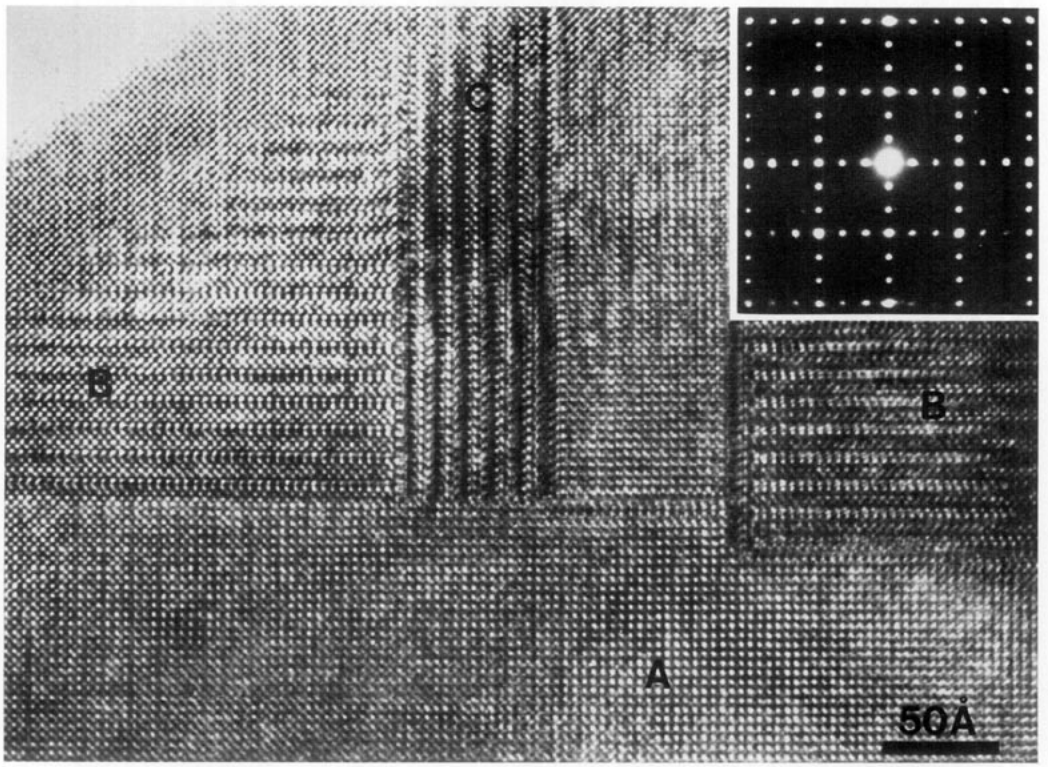

FIG. 5. HREM image along a cubic zone of the perovskite lattice. Twinning on noncoherent {100} planes is regularly observed. The diffraction pattern is shown as an inset.

rial suggest that some more types of defects would occur if an oxygen excess above "O_7" was allowed. The intercalation of an oxygen atom at the boundary between "right" and "left" chains would lead to the formation of three fivefold chain sites for iron, as illustrated in Fig. 2c. This model suggests that even small deviations of the oxygen stoichiometry from "O_7" may induce the formation of a considerable amount of the trigonal–bipyramidal coordination of iron, which can be distinguished in Mössbauer spectra. The formation of these defects would occur during the oxygenation of the orthorhombic phase at small concentrations of extra oxygen atoms, such that the oxygen excess is not yet sufficient for the transition to the tetragonal symmetry.

Furthermore, the material exhibits a remarkable microstructure. In the image of Fig. 4 (see arrows) one notes that the density of antiphase boundaries with a displacement vector along c is surprisingly high. Along such antiphase boundaries (with no pronounced interface plane) chemically different layers are connected through the interface. Since the lattice parameters in $HoSr_2Cu_2(Fe_{0.95}Ga_{0.05})O_{7-\delta}$ are such that $c/6$ equals approximately the a_{123} lattice parameter, orientation variants with mutually perpendicular c-axes occur regularly. Figure 5 shows the high-resolution image along a cubic zone of the perovskite lattice; the pseudo-fourfold symmetric diffraction pattern is shown as an inset. In region A, the c-axis of the triperovskite structure is parallel to the incident beam, whereas it is perpendicular to the incident beam in B and C. A magnified image of the contact layer between two variants shows the perfect continuity of the lattices. This twinning mode of the 123 structure on a noncoherent (100) contact plane was described earlier in oxygen-deficient $YBa_2Cu_3O_{7-\delta}$ (18).

The frequent occurrence of noncoaxial twins and of antiphase boundaries with a displacement vector R = 1/3 [001] can be understood since the unit cell is very close to be composed of the stacking of three cubes, a slight orthorhombicity being only caused by the chain formation in the FeO-plane. Such a geometry allows the perfect fit of a (010) or (100) plane onto a (001) plane and also allows a perfect fit after a shift parallel to [001] over 1/3 [001]. In particular, the deformed cube of the eight copper atoms (in the CuO_2 layers) around the Ho-ion can also be considered as part of the perpendicular variant (Fig. 6a). Since such twins are formed on growth accident, the nucleation of such a cube may induce noncoaxial twins. The requirement of continuity of a CuO_2 layer through the interface leads to a model of the antiphase boundary, which is in accordance with the observations

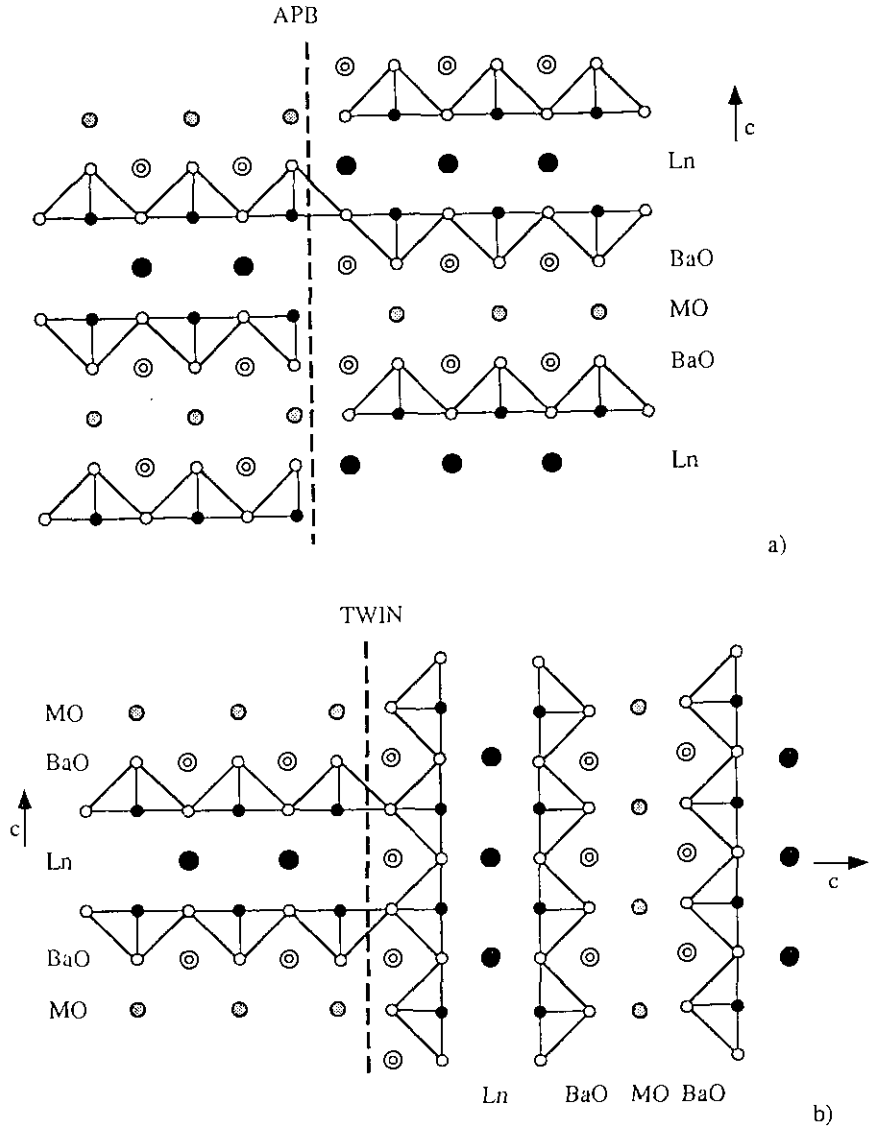

FIG. 6. Schematic representation of the interface structure for (a) an antiphase boundary as imaged in Fig. 4 and (b) a noncoherent twin interface as in Fig. 5.

(Fig. 6b). This model induces the linking of tetrahedral coordinated MO_4 layers with pyramidally coordinated CuO(2) planes. The presence of such interfaces and the mixing of these coordinations is in accordance with the results of Mössbauer spectroscopy, as reported below.

3.2. *Ionic EFG and Hyperfine Field at the Chain Site of Original Ga-Phase* ($HoSr_2Cu_2Ga_{0.97}{}^{57}Fe_{0.03}O_7$)

^{57}Fe Mössbauer probes directly the tetrahedral chain site in the original phase $LnSr_2Cu_2GaO_7$ when the part of iron atoms replacing gallium is small (11). In this work, the sample $HoSr_2Cu_2Ga_{0.97}{}^{57}Fe_{0.03}O_7$ has been measured at 293 and at 4.2 K (Fig. 7). The room temperature spectrum presents an asymmetric quadrupole doublet with a very large quadrupole splitting ($|\Delta E_Q| \approx 1.93$ mm/s). The second quadrupole doublet corresponding to the Cu(2) site has been introduced in the analysis, but its relative abundance does not exceed 3%. The spectrum measured at 4.2 K demonstrates the magnetic ordering involving both Cu(1) and Cu(2) sites. The relative abundance for the second magnetic six-line patterns remains very small and its hyperfine parameters cannot be determined from the present spectra. What is of real interest in these data is the relationship between the quadrupole parameters at 4.2 and at 293 K for the main (97%) subspectrum. The presence of an electric field gradient (EFG) combined with a spontaneous magnetic splitting in the spectrum at 4.2 K can be used to establish the direction of hyperfine field (polar coordinates Θ, ϕ) at the Fe (Ga) site in the

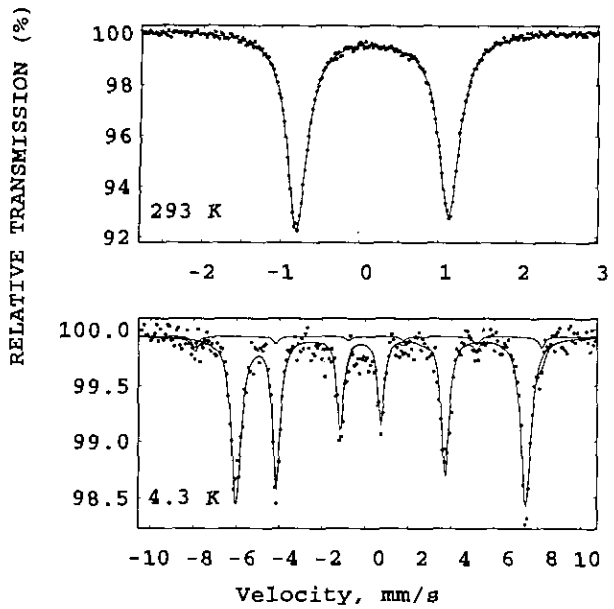

FIG. 7. ^{57}Fe Mössbauer spectra of $HoSr_2Cu_2{}^{57}Fe_{0.03}Ga_{0.97}O_7$ at room temperature and at 4.2 K. The main component (97%) is assigned to a tetrahedral Ga site (Cu(1) site in the "123"-related cuprates).

reference of the principal axes (X, Y, Z) of the electric field gradient (EFG) tensor. In its principal axes, the diagonal EFG tensor is traceless and completely specified by two variables V_{ZZ} and $\eta = (V_{XX} - V_{YY})/V_{ZZ}$, where $|V_{XX}| \leq |V_{YY}| \leq |V_{ZZ}|$ implies an asymmetry parameter η lying between 0 and 1. The point symmetry **m** of the tetrahedral Ga site restricts one of the principal EFG axes to be oriented along the c-axis. We have previously suggested, relying on the structural data (11), that the c-axis component of the EFG tensor is the predominant one (V_{ZZ}), the V_{ZZ} sign being negative due to a strong compression of the GaO_4 (FeO_4) tetrahedron along c. While we arrived at a plausible explanation of the quadrupole spectrum asymmetry due to magnetic perturbations and vibrational anisotropy (11), the actual magnetic ordering investigation had to await the measurements of spectra at 4.2 K. In this regard, the computer fit analysis of the well-resolved magnetic hyperfine sextet is more decisive in deducing both orientations of V_{ZZ} and H. The direction of the iron moments at Cu(1) sites (Ga sites) may allow one to deduce the origin of the magnetic splitting at the diluted ^{57}Fe probe. It is physically plausible that the observed Zeeman splitting is related with the antiferromagnetism of Cu(2) layers which would require the local field to be directed in the basal plane. If the iron moments at the Cu(1) are coupled antiferromagnetically with the copper spins, a value of 90° for Θ is implied for the Cu(1) sites from the requirement of V_{ZZ} to be along the c-axis.

The experimental spectrum at 4.2 K is consistent with these expectations. Because of the large quadrupole lineshift in the Cu(1)-subspectrum, the simple account for the quadrupole energy as a first-order perturbation to the magnetic energy was found to be inappropriate for the spectra processing. Particularly, the theoretical spectrum to the first order of perturbation failed in describing the internal lines (3–4) of the experimental six-line spectrum. The goodness of the fit has been significantly improved using either the exact solution for line positions and line intensities or the solution to the second order of perturbation. These two approaches gave similar results in many spectra, studied in this work.

In the first method, the line positions were computer-fitted (19) to the transition energies determined from numerical diagonalization of the combined Hamiltonian including both magnetic dipole and electric quadrupole interactions. The parameters H, ΔE_Q, Θ, η, and ϕ involved in the formulations for the eigenvalues and eigenvectors for both ground and excited states were allowed to be varied simultaneously or separately in the fit procedure. The dependence of the quality of the fit on the values of initial parameters was examined in several runs of the data processing. The best fit to the data is shown on the Fig. 7, and the refined values are listed in the Table 2.

It is worth noting that the simultaneous variations of η and ϕ in the fit procedure does not lead to an unique stable solution due to the strong correlation between these variables. To clarify the origin of such a correlation and make sure the determination of the refined values by choice of the lowest χ^2 solution, the second method of fit was used assuming Lorentzians for Zeeman sextet lines, located at six independently fitted positions L_1–L_6:

The second-order quadrupole perturbed Zeeman spectrum with quadrupole energy $\Delta E_Q = e^2qQ/2$ and hyperfine field H is composed of six lines with energies (relative to the isomer shift as origin):

$$\begin{aligned} L_1 &= \delta_{IS} - \gamma_1 H + \varepsilon - \xi \\ L_2 &= \delta_{IS} - \gamma_2 H - \varepsilon + \zeta \\ L_3 &= \delta_{IS} - \gamma_3 H - \varepsilon - \zeta \\ L_4 &= \delta_{IS} + \gamma_3 H - \varepsilon + \zeta \\ L_5 &= \delta_{IS} + \gamma_2 H - \varepsilon - \zeta \\ L_6 &= \delta_{IS} + \gamma_1 H + \varepsilon + \xi, \end{aligned} \qquad [1]$$

Here $\gamma_1 = 0.5$, $\gamma_2 = 0.2895$, and $\gamma_3 = 0.07894$ are constants for the Zeeman subspectrum bringing H into velocity scale (1 mm/s $\approx$ 3.1 T), ε is the first-order quadrupole lineshift,

$$\varepsilon = (\Delta E_Q/4)(3\cos^2\Theta - 1 + \eta \sin^2\Theta \cos(2\phi)), \qquad [2]$$

and ξ and ζ are assigned to the second-order quadrupole lineshifts given, for instance, in Ref. (20). It follows from

TABLE 2

Isomer Shifts δ_{IS} (with Respect to Iron Metal at 293 K) and Quadrupole Splittings ΔE_Q for the Cu(1) Site (Ga Site) in $HoSr_2Cu_2Fe_{0.03}Ga_{0.97}O_7$ at 293 K and at 4.2 K

Temperature (K)	δ_{IS}(mm/s) ± 0.002 mm/s	ΔE_Q(mm/s) ± 0.004 mm/s	H_{eff}(T) ± 0.1 T	η ± 0.1	Θ(°)	ϕ(°) ± 10°
293	0.163	−1.928	0.3	0.38	90	49
4.2	0.259	−1.934	40.7			

Note. η is the asymmetry parameter; Θ and ϕ are the polar coordinates of the hyperfine field in the reference of the principal EFG axes.

[1] that the difference of the spacings between the two right-most (5–6) and two left-most (1—2) lines of the six-line spectrum approximated to the second order of quadrupole perturbation is exactly the same as in the first-order approximation and equal to 4ε. On the contrary, the usual first-order determination of field H (in mm/s) as a spacing between the right-most (6) and the left-most (1) lines is not correct if $\xi \neq 0$. Indeed, the first-order approach gave the H value of 42.0 T for the sample $HoSr_2Cu_2Ga_{0.97}Fe_{0.03}O_7$ at 4.2 K, while the correct value is 40.7 T. When the hyperfine field decreases at rising temperature, this discrepancy ($\approx 2\xi$) rapidly increases.

The simple relation [2] allows for the results given in the Table 2 to be independently checked. The comparison of the 4ε value, determined as $(L_6\text{-}L_5)\text{-}(L_2\text{-}L_1)$, with the quadrupole splitting ΔE_Q measured above T_N shows no significant difference between these values. Taking into account the negative sign of ΔE_Q and $\Theta = 90°$, it follows from [2] that $\eta \cos(2\phi) \approx 0$ and either $\eta \approx 0$, or $\phi \approx 45°$. Care must be taken to choose between these possibilities because of the weak sensitivity of the line positions to the variation of either η or ϕ if $\eta \cos(2\phi) \approx 0$. Though the best fit (Table 2) favors the choice of the solution $\phi \approx 45°$, the small value of η may make difficult the accurate determination of the ϕ angle.

As independent evaluation of η has further been performed, using EFG results in a point charge approach, by the method described in Ref. (6). The geometry of the GaO_4 tetrahedron in the structural model, described by Roth *et al.* (8) for $YSr_2Cu_2GaO_7$ differs from that considered previously for FeO_4 in Fe-doped $YBa_2Cu_3O_7$ (21). First, two apical oxygens O_a are separated by a distance of 3.39 instead of 3.64 Å. Second, the displacement **u** of the Fe cation from the apex projection $(O_a)_p$ on the basal plane inward the tetrahedron is 0.7 Å, to be compared with the lower values considered previously: $\mathbf{u} < 0.16$ (22), $\mathbf{u} < 0.4$ (6). Interestingly, the angle $O_p\text{-}(O_a)_p\text{-}O_p$ formed in the basal plane by two oxygens with the axis connecting two apices is 80°, i.e., at midway between a 90°-value for an usual pseudotetrahedral geometry (21) and ≈70° for an ideal tetrahedron. In this geometry, an account for a monopolar ionic contribution into EFG leads to an η value of 0.5–0.6 and ΔE_Q = 1.5–2 mm/s. Another result of EFG calculation is the V_{XX} and V_{YY} directions, parallel and perpendicular, respectively, to the edge of the FeO_4 tetrahedron, lying in the basal plane. A nonzero value of the asymmetry parameter ($\eta = 0.25 \pm 0.1$) was also derived recently from Ga-spin echo spectra (10). Wittmann's calculations for closely related brownmil-

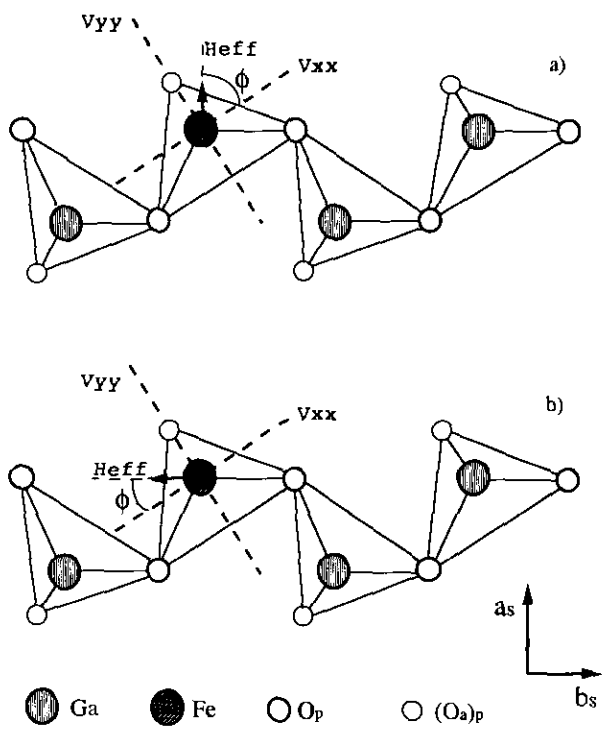

FIG. 8. Proposed spin directions in the chain site of $LnSr_2Cu_2Ga_{1-x}Fe_xO_7$: (a) hyperfine field is in the basal plane and directed along chains; (b) hyperfine field is in the basal plane and directed transverse to the chains. Ga and Fe cations and planar oxygens O_p at the Cu(1) level are depicted, as well as the projections of the apical oxygens on the basal plane $(O_a)_p$.

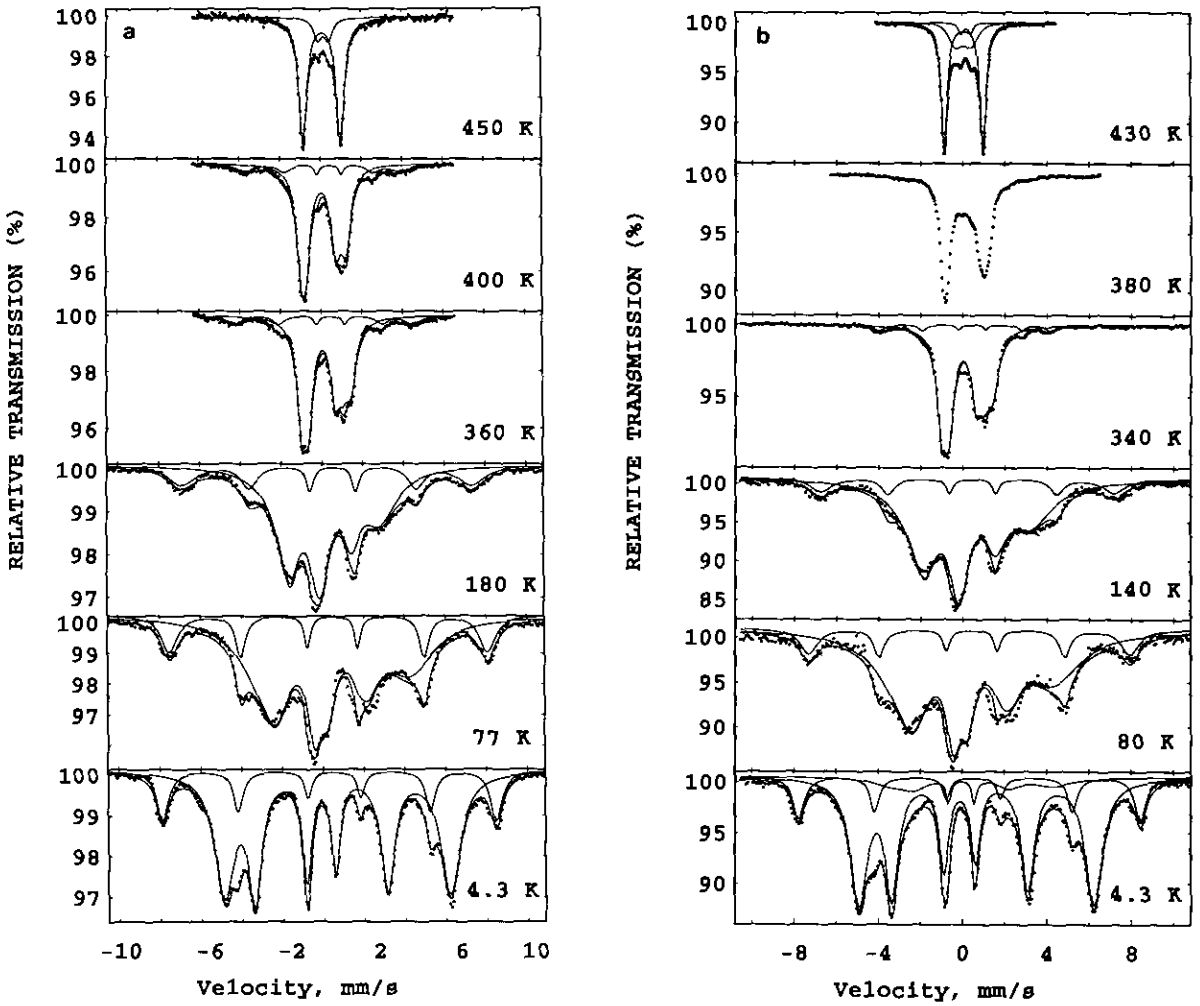

FIG. 9. ^{57}Fe Mössbauer spectra for two samples of $HoSr_2Cu_2Fe_{0.9}Ga_{0.1}O_7$ at different temperatures: (a) Sample [Ar_{fc}] (fast cooled). Two components in the spectra are assigned to Cu(1) and Cu(2) sites according to Table 3. (b) Sample [Ar_{sc}] (slowly cooled). Three components in the spectra are assigned to two Cu(1) sites (tetrahedral one and pyramidal one) and one Cu(2) site according to Table 3. The deconvolution of the spectra into three components is shown for $T = 4.2$ K and for $T = 430$ K. For the sake of clarity, the third subspectrum originating from the Cu(1) pyramidal site is not represented in the deconvolution of spectra measured at intermediate temperatures.

lerite-type oxides $Ca_2Fe_2O_5$ and Ca_2FeAlO_5 having similarly distorted FeO_4 tetrahedra showed that the EFG is also slightly asymmetric ($\eta \approx 0.4$) in the tetrahedral site (23). In a series of tentative fits for $HoSr_2Cu_2Ga_{0.97}Fe_{0.03}O_7$, the fixed values $\phi = 0°$ or $\phi = 90°$ gave very poor goodness of fit even with very small asymmetry ($\eta \approx 0.1$). Therefore, the solution $\eta \approx 0$ seems to be inadequate in agreement with its accidental character, whereas the solution $\cos(2\phi) \approx 0$ is rather correct; i.e., H is about 45° relatively to V_{XX}. This results suggests that the spin direction is either parallel or perpendicular to the chains of tetrahedra, assuming that V_{XX} is nearly along the O_p–O_p axis, as it follows from the calculation of the monopolar contribution to the EFG. Figure 8 shows two corresponding directions of spins in the Cu(1) site. These two variants will be discussed in connection with arrangement of the spins in the magnetic chains observed further in iron-rich compounds. It is noteworthy, that the V_{ZZ} direction parallel to the c-axis in $HoSr_2Cu_2Ga_{0.97}Fe_{0.03}O_7$ is the same as in Fe-doped "YBCO"; the analysis given in a recent paper (24), where V_{ZZ} has erroneously been interpreted to be lying in the basal plane because of a mistake in referring a set of lattice axes, should be revised. This misleading assumption caused also an error in the determination of spin direction (24).

3.3. *Magnetic Order in Chains and Planes of the Iron-Rich Phase $LnSr_2Cu_2Ga_{1-x}Fe_xO_7$($Ln$ = Y, Ho; $x \approx 1$)*

Among the compounds located at the iron-rich end of the solid solution $LnSr_2Cu_2Ga_{1-x}Fe_xO_7$, the samples prepared in an Ar flow are the most interesting because they exhibit

TABLE 3
Quadrupole Splittings ΔE_Q and Saturation Hyperfine Fields H_s for Both Cu(1) and Cu(2) Sites in Two Samples $HoSr_2Cu_2Fe_{0.9}Ga_{0.1}O_7$

Treatment	Site	ΔE_Q[a] (mm/s)	Saturation field H_s(T) ± 0.1 T	η ± 0.05	Θ(°)	ϕ(°) ± 10°	Site occupancy (%) ± 3%
[Ar_{fc}]	Cu(1)	−1.82 ± 0.01	33.5	0.11	90[b]	34	80
	Cu(2)	0.6 ± 0.1	50.7	0.0	>70	Undefined	20
[Ar_{sc}]	Cu(1)[c]	−1.84 ± 0.01	33.2	0.12	90[b]	36	76
	Cu(1)[d]	1.2 ± 0.1	24.0	0.0[a]	0[b]	—	10
	Cu(2)	0.6 ± 0.1	50.4	0.0	>70	Undefined	14

Note. η is the asymmetry parameter; Θ and ϕ are the polar coordinates of the hyperfine field direction in the reference of principal EFG axes. The spectra were measured at the different temperatures shown in Fig. 9 and treated consistently with the same set of ΔE_Q, η, Θ, and ϕ.

[a] The value of ΔE_Q was determined from the spectra above T_N and then fixed to fit the spectra below T_N.

[b] Fixed value.

[c] Tetrahedral coordination.

[d] Pyramidal coordination. For the sake of clarity, this component is not represented in the figure for intermediate temperatures (Fig. 9b). The values for spectra abundances are determined from the spectrum measured above T_N.

a fair in-chain order of the oxygen atoms at the Cu(1) level leading to an orthorhombic structure. Experimental data showing the orthorhombic-to-tetragonal transition in the [Ar] samples by oxygenation has been previously reported (11). In this work, we focused on the domain of stability of the orthorhombic phase, which turned out to exhibit an unusual magnetic behavior.

The Mössbauer spectra of $HoSr_2Cu_2Fe_{0.9}Ga_{0.1}O_7$ for the two methods of sample preparation [Ar_{fc}] and [Ar_{sc}] are shown in Fig. 9. It is clear that the spectra of the iron-rich samples at 4.2 K are more complex than the spectra of the iron-diluted sample (Fig. 7) due to the occurrence of two, at least, iron sites. The spectra can be interpreted by a superposition of two magnetic six-line patterns exhibiting saturation hyperfine fields H_s measured at 4.2 K. The two values of H_s are almost identical to those observed earlier for $YBa_2Cu_3O_{7-\delta}$ for iron sitting on the Cu(1) and Cu(2) sites (1–3). The high-field component is identified with the pyramidal Cu(2) site of the "123" structure, whereas the low-field sextet corresponds to the Cu(1) site (Ga site) of the "123" structure. The spectra measured at different temperatures can be consistently treated with the same set of ΔE_Q, η, Θ, ϕ parameters for the two sites. The refined values are listed in Table 3, whereas temperature-dependent chemical shifts and hy-

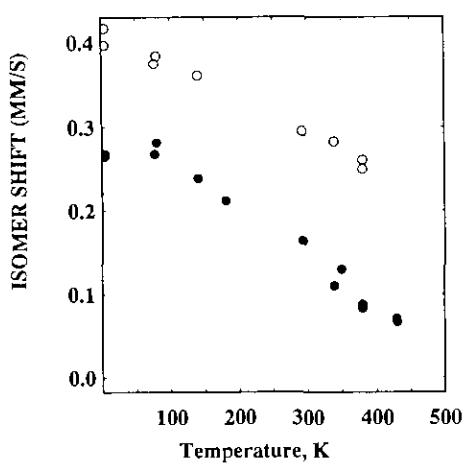

FIG. 10. Temperature dependence of the ^{57}Fe isomer shift for the Cu(1) (filled circles) and Cu(2) (empty circles) sites in $HoSr_2Cu_2Fe_{0.9}Ga_{0.1}O_7$.

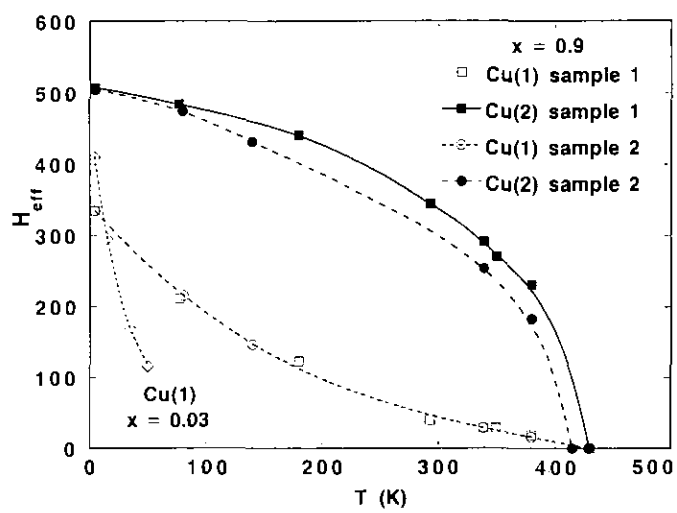

FIG. 11. Temperature dependence of the hyperfine magnetic field in the Cu(1) and Cu(2) sites of two samples of $HoSr_2Cu_2Fe_{0.9}Ga_{0.1}O_7$ (Sample I and Sample II) and in the Cu(1) sites of $HoSr_2Cu_2Fe_{0.03}Ga_{0.97}O_7$. The orthorhombic Samples I and II were prepared in Ar flow by treatments [Ar_{fc}] and [Ar_{sc}], respectively (see text for details of preparation).

perfine field for Cu(1) and Cu(2) sites are shown in Fig. 10 and Fig. 11. While the T-dependence of the chemical shift may be represented by an usual curve for a Debye solid, the magnetic field at the nucleus exhibits a rather unusual behavior.

The structural model implying the presence of some amount of copper atoms in the fourfold coordination (distorted square planar coordination) allows to explain consistently the complex distribution of iron between Cu(1) and Cu(2) sites. A partial occupation of Cu(2) sites by iron is indeed compatible with copper sitting in both Cu(1) and Cu(2) sites. If iron populates the Cu(1) and Cu(2) sites in the approximate proportions 85%: 15%, then the overall stoichiometry of the compound requires 15% of Cu(1) sites to be occupied by copper. Such a high occupancy of Cu(1) sites by copper implies a highly disordered superstructure composed of "left" and "right" chains in agreement with the electron diffraction results.

The comparison of the subspectra intensities for the samples [Ar_{fc}] and [Ar_{sc}] shows that the cooling rate influences the distribution of iron between the Cu(1) and Cu(2) sites. On the other hand, one observes a simultaneous reduction of the magnetic ordering temperature T_N in the slowly cooled sample (Fig. 10), caused, probably, by the presence of doping holes in the Cu(2) layers. Concomitantly with the appearance of holes in the Cu(2) planes, one observes the redistribution of Fe^{3+} and Cu^{2+} ions between planes and chains. In such a situation, the relative charge of the planes with respect to chains may remain the same in the [Ar_{sc}] sample as in the [Ar_{fc}] sample. This suggests that an equilibrium of charge between planes and chains may exist, requiring for some number of holes to be transferred from chains to planes. This model is in agreement with the observation of an efficient transfer of the holes from chains to planes in $YSr_2Cu_2FeO_{7+\delta}$ due to short Cu(2)–O_a bond lengths (13). A small excess of oxygen can be accommodated by [Ar_{sc}] sample with respect to the stoichiometry of the [Ar_{fc}] sample to maintain the charge balance between chains and planes.

The spectrum of the [Ar_{sc}] sample above T_N comprises, at least, three components (Fig. 9b). The major component is related to Fe^{3+} at the tetrahedral bulk site, whereas minor components are related with fivefold coordinations of iron residing at both Cu(1) and Cu(2) sites. The fivefold Cu(1) site arises due to some excess of oxygen with respect to "O_7" stoichiometry. This site is clearly identified in paramagnetic spectra by an isomer shift δ_{IS} of ≈ -0.05 mm/s. The abundance of 10% for this site cannot be neglected in the spectra deconvolution (Table 3), showing that the structural defects associated with a five fold Cu(1) site are encountered frequently in the material. Two mechanisms can be proposed for the incorporation of extra oxygen atoms into the orthorhombic structure in agreement with the Mössbauer and electron diffraction and HREM results. They are both related to the fivefold coordination of iron, that represents a structural defect with respect to an ideal orthorhombic structure of $LnSr_2Cu_2GaO_7$ wherein the oxygen stoichiometry is fixed. The first one deals with the formation of a distorted pyramidal coordination of iron at the antiphase boundary (Fig. 6a) or at the twin boundary (Fig. 6b) between two domains. However, the abundance of the fivefold coordinated Fe on Cu(1) sites in the spectra of the [Ar_{sc}] sample seems to be too large to be produced only by FeO_5 pyramids located at the block interfaces. The defects related to the change from "left" to "right" orientation of the chains could be responsible for the distorted trigonal–bipyramidal FeO_5 configuration at the Cu(1) level (see Fig. 2c). Thus, the relative concentration of both defects is given by the percentage of the weak third component (about 10%) shown in the fit of spectra measured at 4.2 K and above T_N (Fig. 9b).

The oxygen excess is more pronounced for [ArO_{LT} Ar_{LT}] samples. The samples desoxygenated at low temperature [$ArO_{LT}Ar_{LT}$] have been studied and especially for the composition $YSr_2Cu_2Fe_{0.8}Ga_{0.2}O_7$. Figure 12 demonstrates the character of destruction of the magnetic ordering in the presence of holes in the Cu(2) planes for the orthorhombic phase $YSr_2Cu_2Fe_{0.8}Ga_{0.2}O_7$. The first sample ([$Ar_{fc}$]) exhibits a well-defined six-line pattern corresponding to the Cu(2) site, which orders magnetically at 420 K. Though the low-temperature desoxygenation also leads to the formation of the orthorhombic structure in the second sample ([$ArO_{LT}Ar_{LT}$]), it shows some excess of oxygen with respect to "O_7." Consequently, the magnetic order is destroyed far below the characteristic temperature of 420 K, so that this sample is paramagnetic at room temperature. It should be emphasized that no definitive T_N point may be indicated for such a sample due to an intrinsic inhomogenity in the distribution of holes. It is likely that holes are trapped at the walls of the structural domains in the vicinity of intercalated extra oxygen atoms. The structural domains, having different c-axis orientation, were observed by HREM, as shown above. In agreement with HREM evidence, the reflections broadening is observed in the X-ray diffraction pattern of the [$ArO_{LT}Ar_{LT}$] sample, showing that the size of the orthorhombic domains decreases. Due to highly anisotropic magnetic exchange, the structural domains, having different orientations of the c-axis, would coincide with the magnetic domains. When such magnetically independent domains become small ($\approx$50–100 Å) they give rise to superparamagnetic behavior. The blocking temperature of the domains is size-dependent, so that a distribution in size would lead to a progressive decrease of intensity of the six-line Zeeman component, as observed for the Cu(2) site in the [$ArO_{LT}Ar_{LT}$] sample.

In order to better understand the magnetic order in the

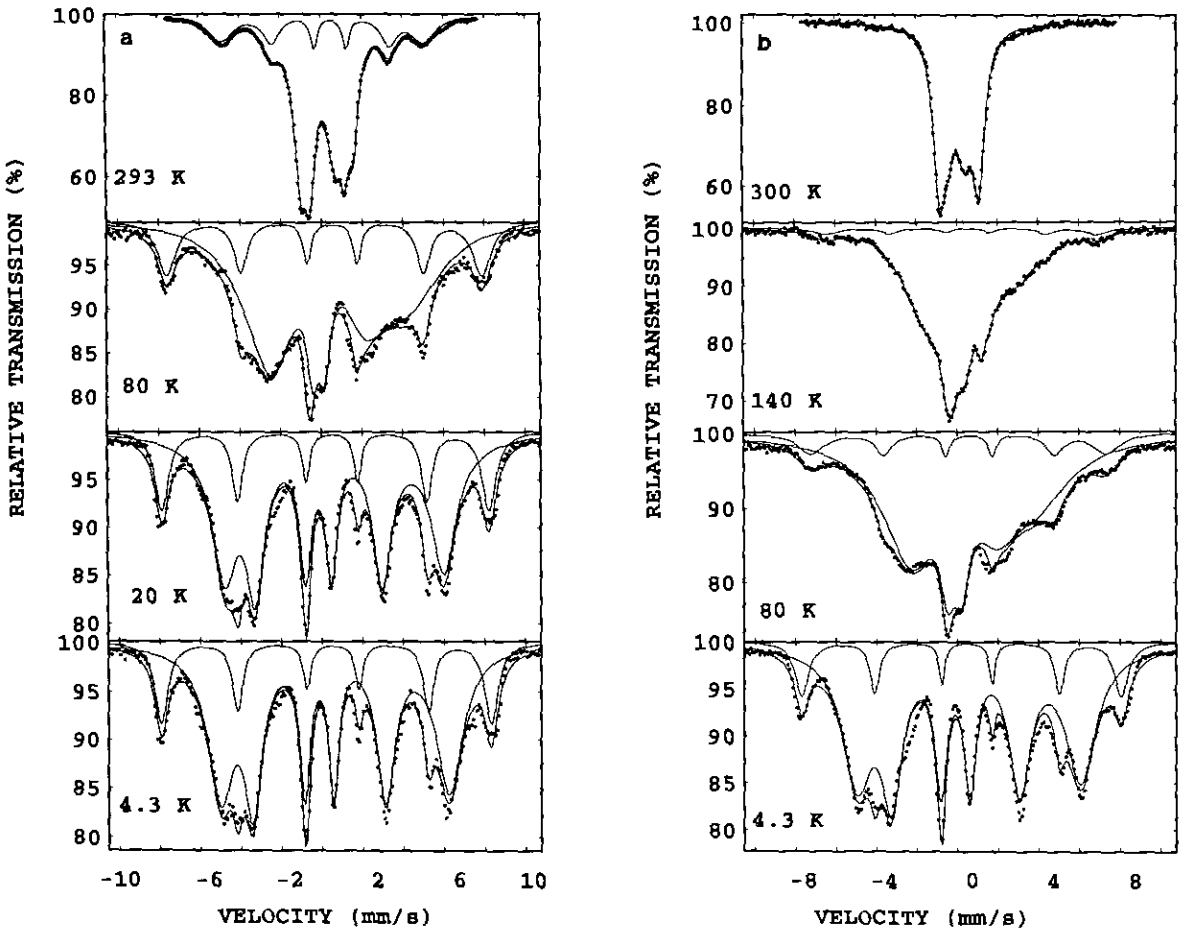

FIG. 12. ^{57}Fe Mössbauer spectra for two samples of $YSr_2Cu_2Fe_{0.8}Ga_{0.2}O_7$, at different temperatures: (a) Sample [Ar_{fc}] (fast cooled in Ar flow). (b) Sample [$ArO_{LT}Ar_{LT}$] (subsequently oxygenated and reduced at low temperature (400°C). Note that the third subspectrum originating from the Cu(1) pyramidal site is not represented in the deconvolution of spectra for clarity.

iron-rich phases, let us compare our results, obtained for $HoSr_2Cu_2Fe_{0.9}Ga_{0.1}O_7$, with those observed for the Fe-doped system $Y_{1-x}Pr_xBa_2Cu_3O_y$ with an iron concentration up to 10% (only 3% in the Cu(2) site (25). Iron located in the Cu(2) site of our samples exhibits a magnetic behavior (Fig. 11), similar to the one of diluted iron probe in Cu(2) site of $YBa_2Cu_3O_6$ (25). In spite of a significant occupancy of the Cu(2) site by iron atoms (up to 10%), neither the shift in T_N induced by Fe impurity, nor changes in the shape of $H(T)$ dependence with respect to the dilution case were observed. This result is coherent with the weakness of the Fe–Cu exchange interaction compared to the Cu–Cu interaction (25). Moreover, since possible Fe–Fe interactions do not affect the character of the magnetic ordering in the Cu(2) sublattice, one can say that the clustering of Fe in the Cu(2) site is not favourable. The substitution of iron for copper at the Cu(2) site influences the magnetic order similarly to a dilution, i.e., less effectively than the introduction of holes into the Cu(2) layer through oxygenation or heterovalent substitution at the Ln site (5).

The most remarkable feature of the T-dependent Mössbauer spectra is an unusual concave down shape of the $H(T)$ curve for the chain site (Fig. 11). The magnetic hyperfine field appears at the Cu(1) site at the same T_N point of 420 K as in the Cu(2) sublattice. Such a behavior suggests a rather weak magnetic coupling between the Cu(1) and Cu(2) sites. Note that the Cu(1) and Cu(2) sublattices were also observed to be coupled in the deoxygenated compound $YBa_2Cu_{2.7}Fe_{0.3}O_{6.36}$, which shows a single magnetic ordering temperature of about 435 K for both sublattices. On the opposite, the Cu(1) and Cu(2) sites order magnetically at different temperatures for lower iron concentrations, such that two ordering temperatures $T_{N1} \approx 20$ K and $T_{N2} \approx 405$ K coexist in $YBa_2Cu_{2.85}Fe_{0.15}O_{6.45}$ (26). Two magnetic ordering temperatures for slightly Fe-doped $YSr_2Cu_2GaO_7$ were also observed (24). The magnetic phase diagram of the $YBa_2Cu_{1-x}Fe_xO_{6.2}$ sys-

TABLE 4
Quadrupole Splittings ΔE_Q and Saturation Hyperfine Fields H_s for Both Cu(1) and Cu(2) Sites in Two Samples $YSr_2Cu_2Fe_{0.8}Ga_{0.2}O_7$

Treatment	Site	ΔE_Q[a] (mm/s)	Saturation field H_s(T) ± 0.1 T	η ± 0.1	θ(°) ± 10°	ϕ(°) ± 10°	Site occupancy (%) ± 3%
$[Ar_{fc}]$	Cu(1)	−1.94 ± 0.01	33.8	0.38	90	37	81
	Cu(2)	0.6 ± 0.1	50.5	0.0 [b]	>70	Undefined	19
$[ArO_{LT}Ar_{LT}]$	Cu(1)[c]	−1.92 ± 0.01	33.0	0.28	90	37	69
	Cu(1)[d]	1.2 ± 0.1[d]	24.0	0.0[b]	0[b]	—	18
	Cu(2)	0.5 ± 0.1	49.1	0.0[b]	>70	Undefined	13

Note. η is asymmetry parameter; Θ and ϕ are polar coordinates of the hyperfine field direction in the reference of principal EFG axes. The spectra were measured at the different temperatures shown in Fig. 12 and treated consistently with the same set of ΔE_Q, η, Θ, and ϕ.

[a] The value of ΔE_Q was determined from the spectra above T_N and then fixed to fit the spectra below T_N.

[b] Fixed value.

[c] Tetrahedral coordination.

[d] Pyramidal coordination. For the sake of clarity, this component is not represented in Fig. 12b. The values for subspectra abundances are determined from the spectrum measured above T_N.

tem studied by Mirebeau *et al.* (7) shows two domains of different magnetic structures with a boundary at $x \approx 0.1$. When $x > 0.1$, the magnetic system exhibits a single ordering temperature, but two transitions appear at temperatures $T_{N1} = 405$ K and $T_{N2} = 50$ K for low iron content ($x < 0.1$). This is explained by the breaking of the interlayer Cu(2)–Cu(2) coupling with occurrence of the magnetic moment at the Cu(1) site.

In the iron-rich compounds with ordered tetrahedral chains like $HoSr_2Cu_2Fe_{0.9}Ga_{0.1}O_7$, the Cu(1) and Cu(2) sublattices can be considered as constituents of the magnetic structure of the well known G-type (27). These sublattices are antiferromagnetic and the intersublattice interactions are likely also antiferromagnetic. Indeed, the strength of the antiferromagnetic coupling as well within Cu(2) and Cu(1) sublattices as between them is related to the cation–anion–angle; it would increase toward linear configuration (27). When the Cu(1) and Cu(2) sites are occupied preferentially by ions Cu^{2+} and Fe^{3+}, then the Cu^{2+}–O^{2-}–Cu^{2+}, Cu^{2+}–O^{2-}–Fe^{3+}, and Fe^{3+}–O^{2-}–Fe^{3+} angles calculated from the structural parameters (9) are, respectively, 166°, 168°, and 125°. These values suggest a similarity of the superexchange interactions in $HoSr_2Cu_2Fe_{0.9}Ga_{0.1}O_7$ and in the classical G-antiferromagnet $Ca_2Fe_2O_5$ when compared with the corresponding angles $[Fe^{3+}]$–O^{2-}–$[Fe^{3+}]$ of 167°, $[Fe^{3+}]$–O^{2-}–(Fe^{3+}) of 147°, and (Fe^{3+})–O^{2-}–(Fe^{3+}) of 132° (here symbols $[Fe^{3+}]$ and (Fe^{3+}) denotes the octahedral and the tetrahedral iron, respectively) (28).

Thus, the analysis of the hyperfine field variation for the Cu(1) and Cu(2) sublattices with temperatures in $HoSr_2Cu_2Fe_{0.9}Ga_{0.1}O_7$ (Fig. 11) shows the leading role of the antiferromagnetic coupling within the Cu(2) sublattice. On the opposite, in this G-structure, the antiferromagnetism of the Cu(1) sublattice has to be essentially reduced due to the weakness of the exchange coupling Fe^{3+}–O^{2-}–Cu^{2+}. No convenient first-order magnetic phase transition is observed for the chain site in spite of exchange interactions Fe^{3+}–O^{2-}–Fe^{3+} between sublattices; this result is in agreement with the well-known fact that no long-range magnetic ordering exists in purely 1D systems (29). The spontaneous magnetisation in the chains at nonzero temperature can be triggered by weak intechain interactions. Kimball *et al.* (30) explained by this phenomenon the magnetic low-temperature transition in the Fe–O–Fe chains for oxygen saturated $YBa_2Cu_{3-x}Fe_xO_{7-\delta}$ with low x values. No magnetic order in the Cu(2) planes exists indeed in such superconducting samples. In the Cu(1) site, the superexchange interactions between neighbouring Fe ions via oxygen ions ensure the intrachain coupling. However, the nature of the interchain coupling is not clear; the low level of Fe substitution requires that Fe–Cu magnetic interactions may also be responsible for the magnetic splitting in such samples (31). When the chains are located between magnetically ordered Cu(2) planes, as in $LnSr_2Cu_2Fe_{0.9}Ga_{0.1}O_7$, then all three Cu–Cu, Fe–Fe, and Cu–Fe interactions are involved to yield the antiferromagnetic G-structure.

It is interesting to compare the spin direction for $LnSr_2Cu_2Fe_{0.9}Ga_{0.1}O_7$ with that of other G-type antiferromagnets. In brownmillerite Ca_2FeAlO_5, the spin orientation along chains of tetrahedra (Fig. 8a) has been observed (32), whereas spins perpendicular to chains (Fig. 8b) have also been found, in particular, in $Ca_2Fe_2O_5$ (33), $Sr_2Fe_2O_5$ (34), $Sr_2Co_2O_5$ (35). Since the Cu(2) antiferromagnetic sublattice is the leading sublattice in $LnSr_2Cu_2Fe_{0.9}Ga_{0.1}O_7$, the spin direction in the Cu(1) site would simply follow the orientation of spin in the Cu(2) planes.

For our iron-rich materials, the ϕ angle in the Cu(1) site is slightly lower than 45°. These values (Tables 3 and 4) are close to the zigzag angle that two planar oxygens O_p–O_p form with the mean chain direction (b_x-axis). This suggests that the spin is oriented rather along the chains in iron-rich compounds. Therefore, the copper spins in the Cu(2) site are also oriented along the b_s axis, that is along the longer axis b_o in the a_ob_o-plane. The same orientation along the longer axis in the basal plane has also been observed by neutron diffraction in the orthorhombic La_2CuO_4 (2). Though the actual spin direction in the Cu(2) planes of tetragonal $YBa_2Cu_3O_6$ is not yet known, the [110] orientation may reflect a general feature of highly anisotropic superexchange interactions in CuO_2 layers.

The most striking result is that the saturation hyperfine field at the chain site of iron-diluted compound $HoSr_2Cu_2Ga_{0.97}Fe_{0.03}O_7$ is considerably higher than in the iron-rich $HoSr_2Cu_2Fe_{0.9}Ga_{0.1}O_7$ and $YSr_2Cu_2Fe_{0.8}Ga_{0.2}O_7$ compounds. Felner *et al.* (24) also observed a rather high H_s value of 42.0 T in $YSr_2Cu_2GaO_7$ with a diluted ^{57}Fe Mössbauer probe. On the contrary, the values in the range 30–35 T are typical for tetrahedral iron located at the Cu(1) level in Fe-doped $YBa_2Cu_3O_{7-y}$. The most plausible explanation of such a difference is related with the fact that iron does not form the chains in the diluted system $LnSr_2Cu_2Ga_{1-x}Fe_xO_7$ ($x \approx 0.03$). The tetrahedral coordination in the host matrix $YSr_2Cu_2GaO_7$ is fairly well accommodated by iron, so that the latter does not exhibit any clustering. Therefore, iron experiences an exchange field due to Fe–Cu coupling only. By contrast, it is well accepted that iron forms linear clusters in the host matrix $YBa_2Cu_3O_{7-y}$ (22, 30, 36), as well as fairly perfect chains of tetrahedra in $LnSr_2Cu_2Ga_{1-x}Fe_xO_7$ ($x \approx 0.9$). In this case, the Fe–Fe exchange interactions would be the strongest ones. The linear $(Fe–O)_n$ chains render overall magnetic system to be essentially one-dimensional. This may explain the zero-point reduction of spin due to fluctuations in 1D magnetic system (37).

4. CONCLUDING REMARKS

The richness of the ^{57}Fe hyperfine structure in the cuprate superconductors makes the Mössbauer spectroscopy an important tool for studying either iron substitution effects on the structure and properties of cuprates or generic magnetic effects associated with CuO_2 planes. Considerable progress in this area has already been done by a systematic examination of the peculiar hyperfine components due to Fe species in specific coordinations, realised in specially synthesized "model" compounds. For instance, in the "123"-related cuprates, the Mössbauer response of either pyramidal coordination of iron in the Cu(2) site, or tetrahedral coordination of iron in the Cu(1) site has been isolated (6, 11, 38). Furthermore, the iron driving from Cu(1) to Cu(2) sites performed previously in $Y_{1-z}Ca_zBa_2Cu_{3-x}Fe_xO_{7-y}$ (38) provided an important insight on the magnetic spin-glass effects resulting from iron sitting in the Cu(2) planes (6). The Fe substitution for Ga in $LnSr_2Cu_2GaO_7$ allowed an examination of Fe quadrupole interaction and vibrational anisotropy in such a site (11). This study performed on the same model system $LnSr_2Cu_2Ga_{1-x}Fe_xO_{7-\delta}$ provides a better understanding of the magnetic interactions between CuO_2 planes and FeO tetrahedral chains. The results obtained on the local field direction in both Cu(1) and Cu(2) sites are in harmony with the spin orientation in the basal plane, as would be required by the known antiferromagnetic structures.

ACKNOWLEDGMENTS

We thank Professor S. Amelinckx (RUCA) for stimulating discussions on the structural aspects of some of the materials investigated. This work has been partly supported by Ministry of Research and Technology of France and Russian Council on high-T_c superconductivity.

REFERENCES

1. Yu. T. Pavlukhin, N. G. Hainovsky, Y. Y. Medikov, and A. I. Rykov. *Int. J. Mod. Phys. B* **3,** 711–717 (1989).
2. P. Boolchand and D. McDaniel, *in* "Studies on High-Temperature Superconductors" ed. (A. V. Narlikar, Ed.), Vol. 4, p. 143. (Nova Science, New York, 1990).
3. I. S. Lyubutin, V. G. Terziev, T. V. Dmitrieva, S. V. Luchko, and A. Ya. Shapiro, *Solid State Commun.* **86,** 651 (1993).
4. I. Nowik and I. Felner, *Mod. Phys. Lett. B* **5,** 273 (1991).
5. H. Casalta, H. Alloul, and J.-F. Marucco, *Physica C* **204,** 331 (1993).
6. A. Rykov, A. Ducouret, N. Nguyen, V. Caignaert, F. Studer, and B. Raveau, *Hyperfine Interact.*, **77,** 227 (1993).
7. I. Mirebeau, C. Bellouard, M. Hennoin, V. Caignaert, and E. Suard, *J. Appl. Phys.* **73,** 5689 (1993).
8. G. Roth, P. Adelmann, G. Heger, R. Knitter, and Th. Wolf, *J. Phys. I.* **1,** 721 (1991).
9. J. T. Vaughey, J. T. Thiel, E. F. Hasty, D. A. Groenke, Ch. H. Stern, K. R. Poepelmeier, B. Dabrowski, D. G. Hinks, and A. W. Mitchell, *Chem. Mater.* **3,** 935 (1991).
10. M. W. Pieper, *Physica C* **190,** 261 (1992).
11. A. Rykov, V. Caignaert, and B. Raveau, *J. Solid State Chem.* **109,** 295, (1994).
12. M. Pissas, G. Kallias, A. Simopoulos, D. Niarchos, and A. Kostikas, *Phys Rev. B* **46,** 14119 (1992).
13. M. G. Smith, R. D. Taylor, and J. D. Thompson, *Physica C* **208,** 91 (1993).
14. Q. Huang, R. J. Cava, A. Santoro, J. J. Krajewski, and W. F. Peck, *Physica C* 193, 196 (1992).
15. O. Milat, T. Krekels, G. Van Tendeloo, and S. Amelinckx, *J. Phys. I. France* **3,** 1219 (1993).
16. O. Milast, T. Krekels, and S. Amelinckx, submitted for publication.
17. T. Krekels, O. Milat, G. Van Tendeloo, S. Amelincks, T. G. N. Babu, A. J. Wright, and C. Greaves, *J. Solid State Chem.*, in press.
18. H. W. Zandbergen, G. Van Tendeloo, T. Okabe, and S. Amelinckx, *Phys. Status Solidi, A* **103,** 45–72 (1987).
19. J. Teillet, and F. Varret, MOSFIT programme. [unpublished]
20. M. Eibshütz and M. E. Lines, *Phys. Rev. B* **25,** 4256 (1982).
21. M. E. Lines and M. Eibschutz, *Physica C* **166,** 235–247 (1990).

22. B. D. Dunlap, J. D. Jorgensen, C. Segre, A. E. Dwight, J. L. Matykiewicz, H. Lee, W. Peng, and C. W. Kimball, *Physica C* **158,** 397 (1989).
23. F. Wittmann, *Phys. Lett.* **24A,** 252 (1967).
24. I. Felner, I. Nowik, U. Asaf, G. Yona, U. Yaron, and E. R. Bauminger, *Physica C* **210,** 55 (1993).
25. I. Nowik, G. Kaindl, E. R. Bauminger, I. Felner, M. Kowitt, and U. Yaron, *Solid State Commun.* **74,** 957 (1990).
26. I. S. Lyubutin, V. G. Terziev, T. V. Dmitrieva, A. M. Balagurov, and S. Nasu, *Physica C* **195,** 383 (1992).
27. E. F. Bertaut, *in* "Magnetism" (Rado and Shul, Eds.), Vol. III, p. 149. Academic Press, New York, 1963.
28. S. Geller, R. W. Grant, U. Gonser, H. Wiedersich, and G. P. Espinosa, *Phys. Lett.* **20,** 115 (1966).
29. L. J. de Jongh and A. R. Miedema, *Adv. Phys.* **23,** 1 (1974).
30. C. W. Kimball, B. Dabrowski, Yu. Liang, W. Peng, B. D. Dunlap, *Hyperfine Interact.* **72,** 153 (1992).
31. S. Suharan, C. E. Johnson, Q. A. Pankhurst, and M. F. Thomas, *J. Magn. Magn. Mater.* **104–107,** 879 (1992).
32. R. W. Grant, S. Geller, H. Wiedersich, and L. D. Fullmer, *J. Appl. Phys.* **39,** 1122 (1968).
33. Z. Friedman, H. Shaked, and S. Shtrikman, *Phys. Lett.* **25A,** 9, (1967).
34. T. Takeda, Y. Yamaguchi, H. Watanabe, S. Tomiyoshi, and H. Yamamoto, *J. Phys. Soc. Jpn.* **26,** 1320 (1969).
35. T. Takeda, Y. Yamaguchi, and H. Watanabe, *J. Phys. Soc. Jpn.* **33,** 970 (1972).
36. P. Bordet, J. L. Hondeau, P. Strobel, M. Marezio, and A. Santoro, *Solid State Commun.* **66,** 435 (1988).
37. P. W. Andersen, *Phys. Rev.* **86,** 694 (1952).
38. A. Rykov, V. Caignaert, N. Nguyen, A. Maignan, E. Suard, and B. Raveau, *Physica C* **205,** 63 (1993).